Supporting Information

Effects of Hydrofluoric Acid Concentration on the Density of Silanol Groups and Water Adsorption in Hydrothermally Synthesized Transition Metal Substituted Silicalite-1

Daniel T. Bregante, David Potts, Ohsung Kwon, E. Zeynep Ayla,

Jun Zhi Tan, and David W. Flaherty*

Department of Chemical and Biomolecular Engineering

University of Illinois at Urbana-Champaign, Urbana, IL 61801, USA

*Corresponding Author

Phone: +1 217-244-2816

Email: dwflhrty@illinois.edu

S1. X-Ray Diffraction

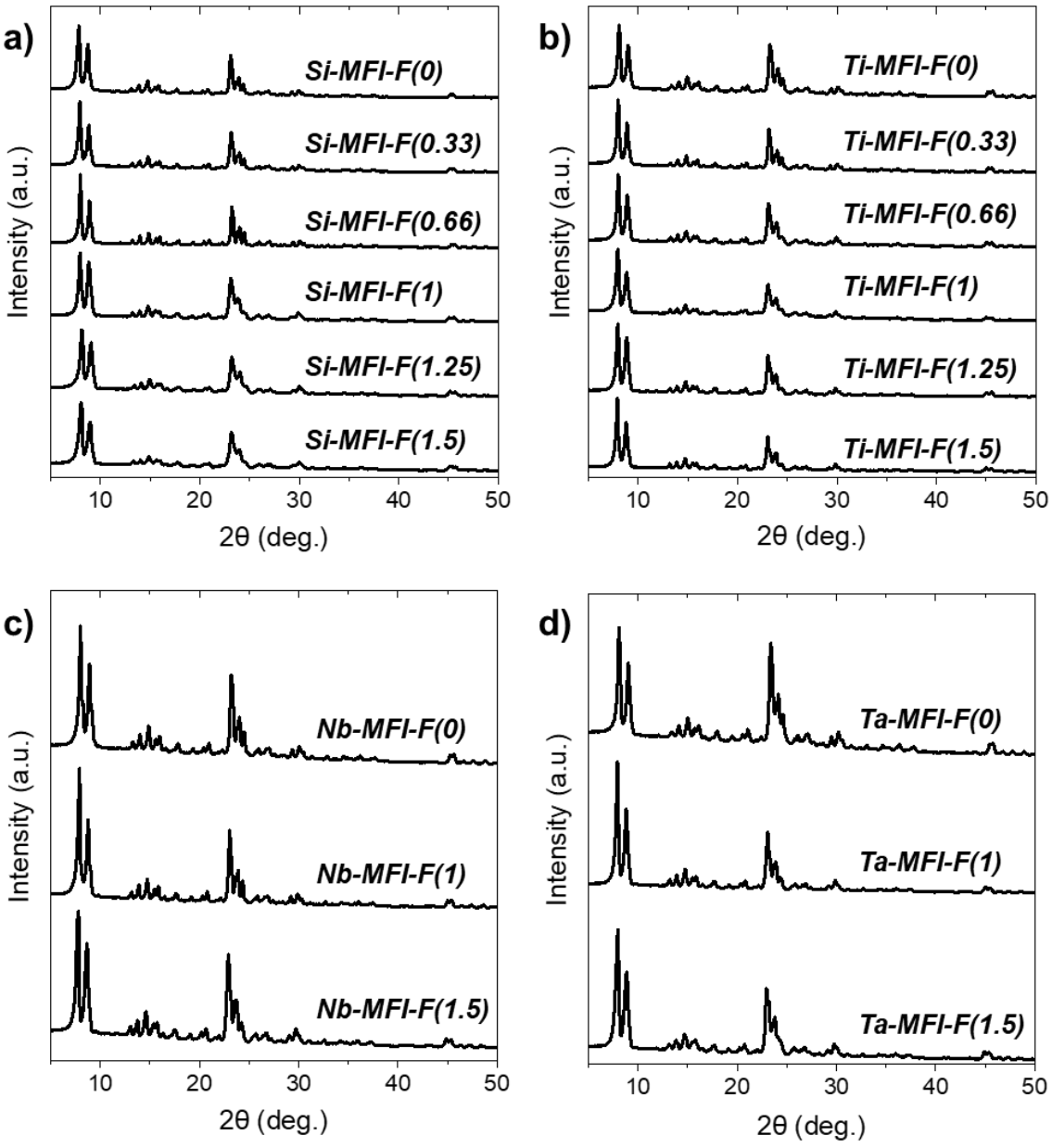

Figure S1. X-ray diffractograms for a) Si-MFI-F(x), b) Ti-MFI-F(x), c) Nb-MFI-F(x), and Ta-MFI-F(x). Diffractograms are vertically offset for clarity.

Figure S1 shows X-ray diffractograms for all M-MFI-F(x) discussed within this study. All diffractograms possess diffraction patterns that are indicative of the MFI framework.

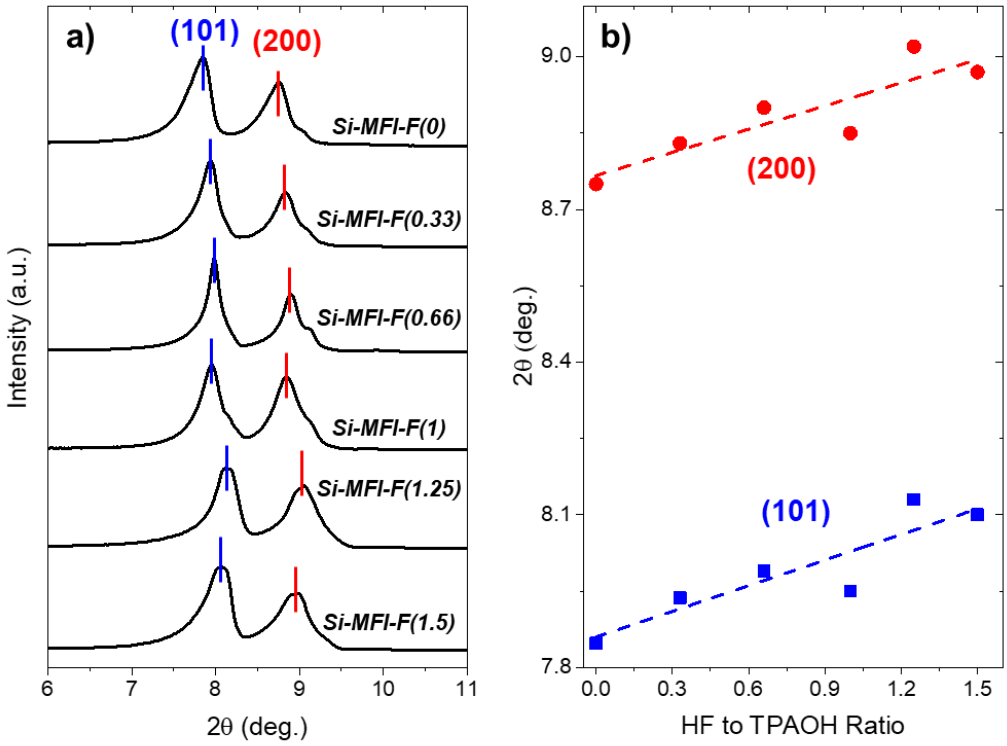

Figure S2. a) X-ray diffractograms for Si-MFI-F(x) and b) diffraction peak centers for (101) and (200) reflections as a function of HF to TPAOH ratio. Diffractograms are vertically offset for clarity. Dashed lines in panel b) represent linear fits.

Figure S2 shows that X-ray diffraction peaks for the (101) and (200) reflections within Si-MFI-F(x) increase monotonically with the HF:TPAOH ratio, by a value of 0.2 degrees between Si-MFI-F(0) and Si-MFI-F(1.5). The diffraction peaks that correspond to the (101) and (200) reflections[1] of MFI at ~8 and ~9 degrees decrease monotonically as the HF:TPAOH ratio decreases and span a range of 0.2 degrees between HF to TPAOH ratios of 1.5 and zero. The shift in diffraction peak positions to lower angles with an increase in SiOH density suggests that the hydrogen bonding interactions among -OH functions in framework vacancies slightly expand the unit cell of MFI relative to the defect-free structure.[2-3]

S2. Diffuse Reflectance UV-vis Spectra

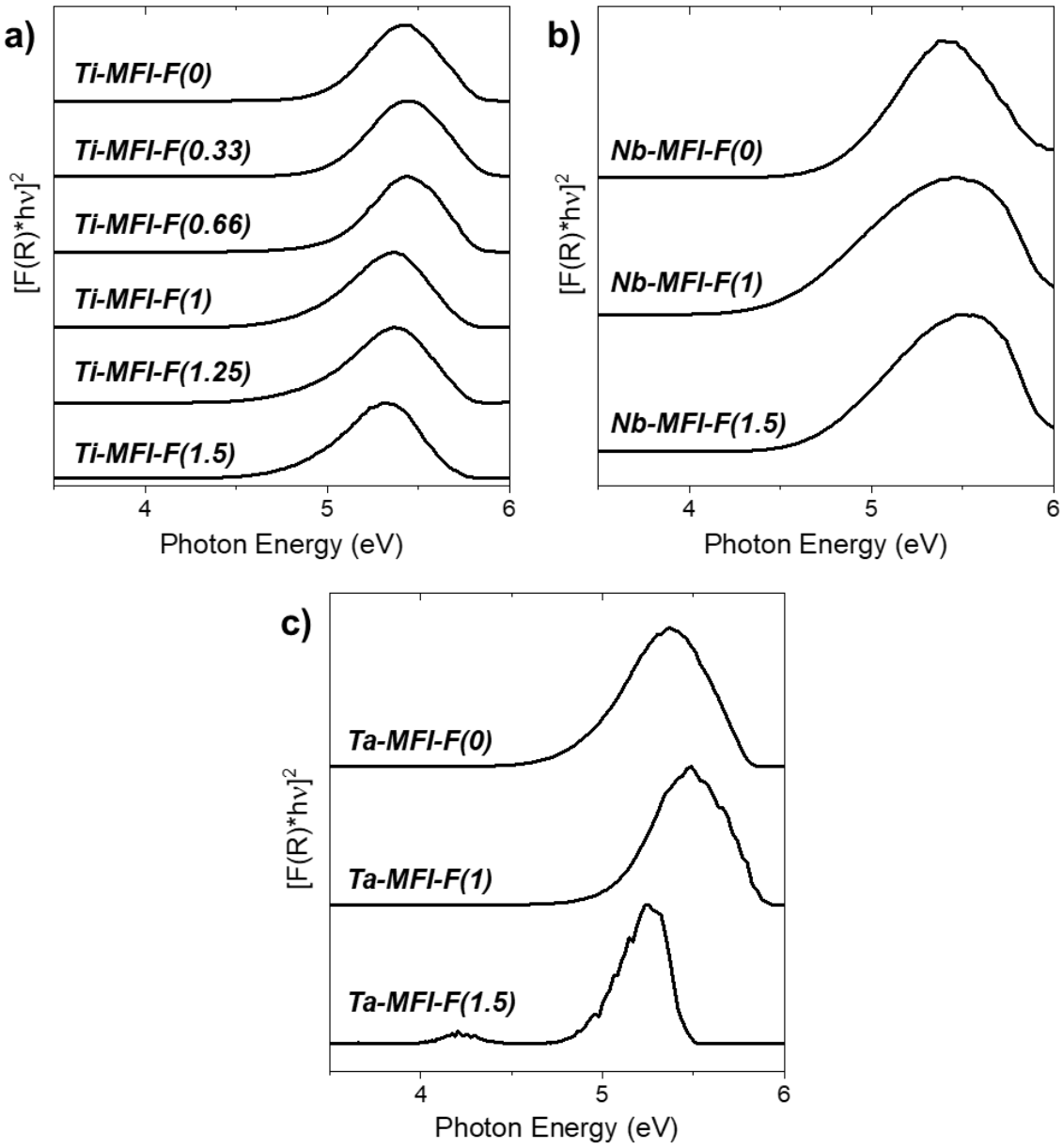

Figure S3. Tauc plots for a) Ti-MFI-F(x), b) Nb-MFI-F(x), and c) Ta-MFI-F(x). All plots were normalized to the most intense feature around 5.2 eV and are vertically offset for clarity.

Figure S3 shows that, with the exception of Ta-MFI-F(1.5), all M-MFI-F(x) contain a single UV-vis absorbance feature around 5.2 eV. The small absorbance feature at 4.2 eV for Ta-MFI-F(1.5) corresponds to a small quantity of bulk Ta_2O_5. The leading edge (4.8 – 5.0 eV) for each Tauc plot was fit using a line to extrapolate the x intercept, which is equal to the band gap of the material.

S3. N_2 Adsorption Isotherms over Ti-MFI-F(x)

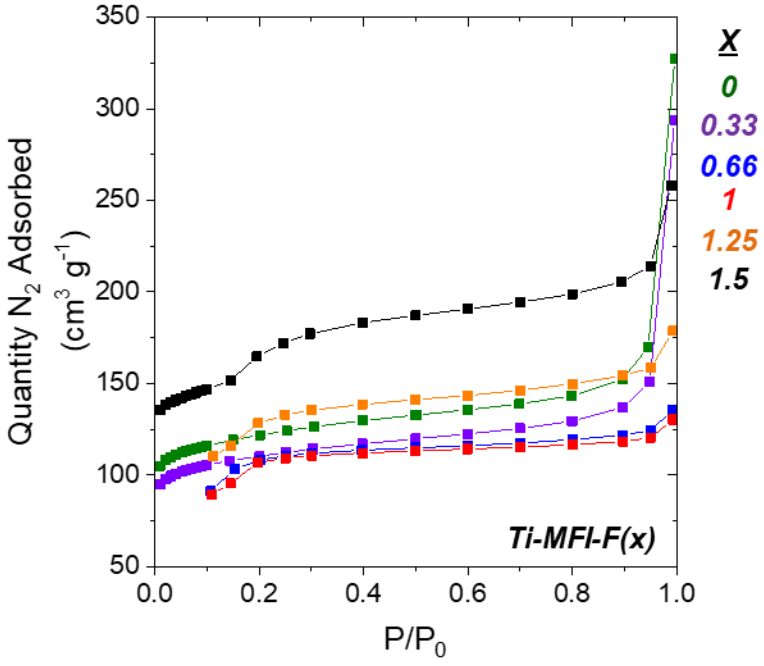

Figure S4. Representative N_2 adsorption isotherms (77 K) over Ti-MFI-F(x) samples.

S4. Infrared Spectra of M-MFI-F(1.5) Materials

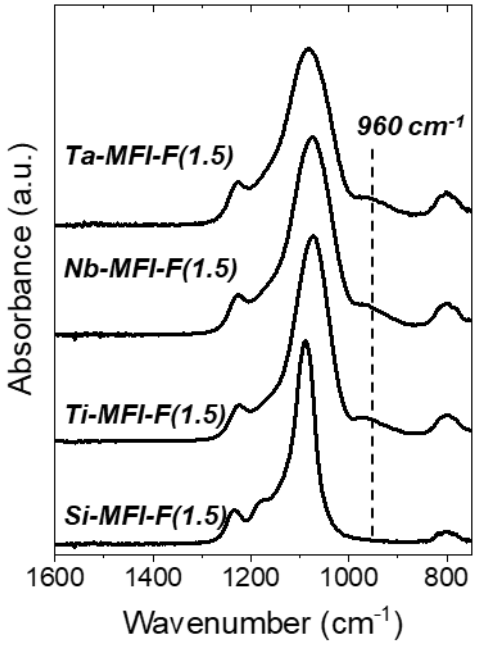

Figure S5. Infrared spectra of Si-, Ti-, Nb-, and Ta-MFI-F(1.5) at ambient conditions. All spectra are normalized to the framework vibration at ~1080 cm^{-1} and are vertically offset for clarity.

S5. Raman Spectra of M-MFI-F(0) and M-MFI-F(1.5) Materials

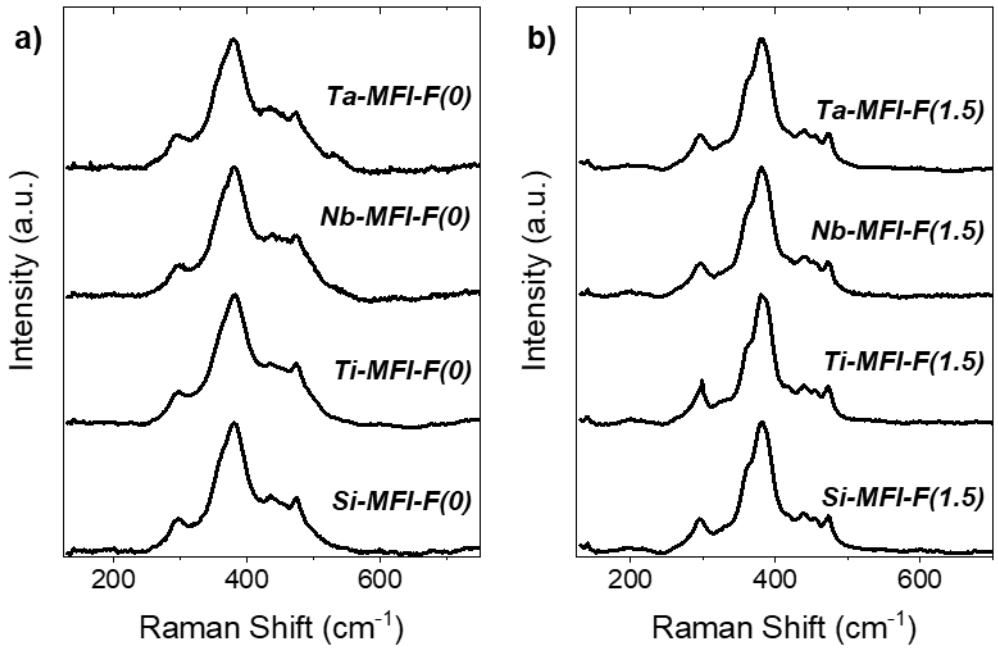

Figure S6. Raman spectra (λ_{ex} = 532 nm) of a) M-MFI-F(0) and b) M-MFI-F(1.5) materials. All features are normalized to the most intense feature and are vertically offset for clarity.

Figure S6 shows Raman spectra of all M-MFI-F(0) and M-MFI-F(1.5) possess vibrational features between 300 – 500 cm^{-1} that is characteristic of the MFI framework.[4] Bulk TiO_2, Nb_2O_5, and Ta_2O_5 possess strong scattering features located at 140,[5] 680,[6] and 250[7] cm^{-1}, respectively. Notably, none of the Raman spectra for Ti-, Nb-, or Ta-bearing MFI materials contain any scattering features that are reminiscent of the corresponding bulk metal oxide domains. Consequently, these data, in conjunction with our ATR-IR measurements (Figure 2) and DRUV-vis spectra strongly suggest that these materials contain predominantly monomeric metal atoms that are substituted into the framework of MFI.

S6. Relationship Between Crystallization Rates and Heteroatom Identity

Empirically, the crystallization time increases with the radius of the metal cation incorporated into the MFI framework (e.g., Si^{4+}(40 pm), Ti^{4+} (56 pm), Nb^{5+} (78 pm), and Ta^{5+} (78 pm))[8] for M-zeolite syntheses.[9] This phenomenon may reflect an expansion of the unit-cell caused by incorporation of the heteroatoms,[2, 10] which in turn, increases the energetic barrier for crystallization.

S7. Infrared Spectra of M-MFI-F(x)

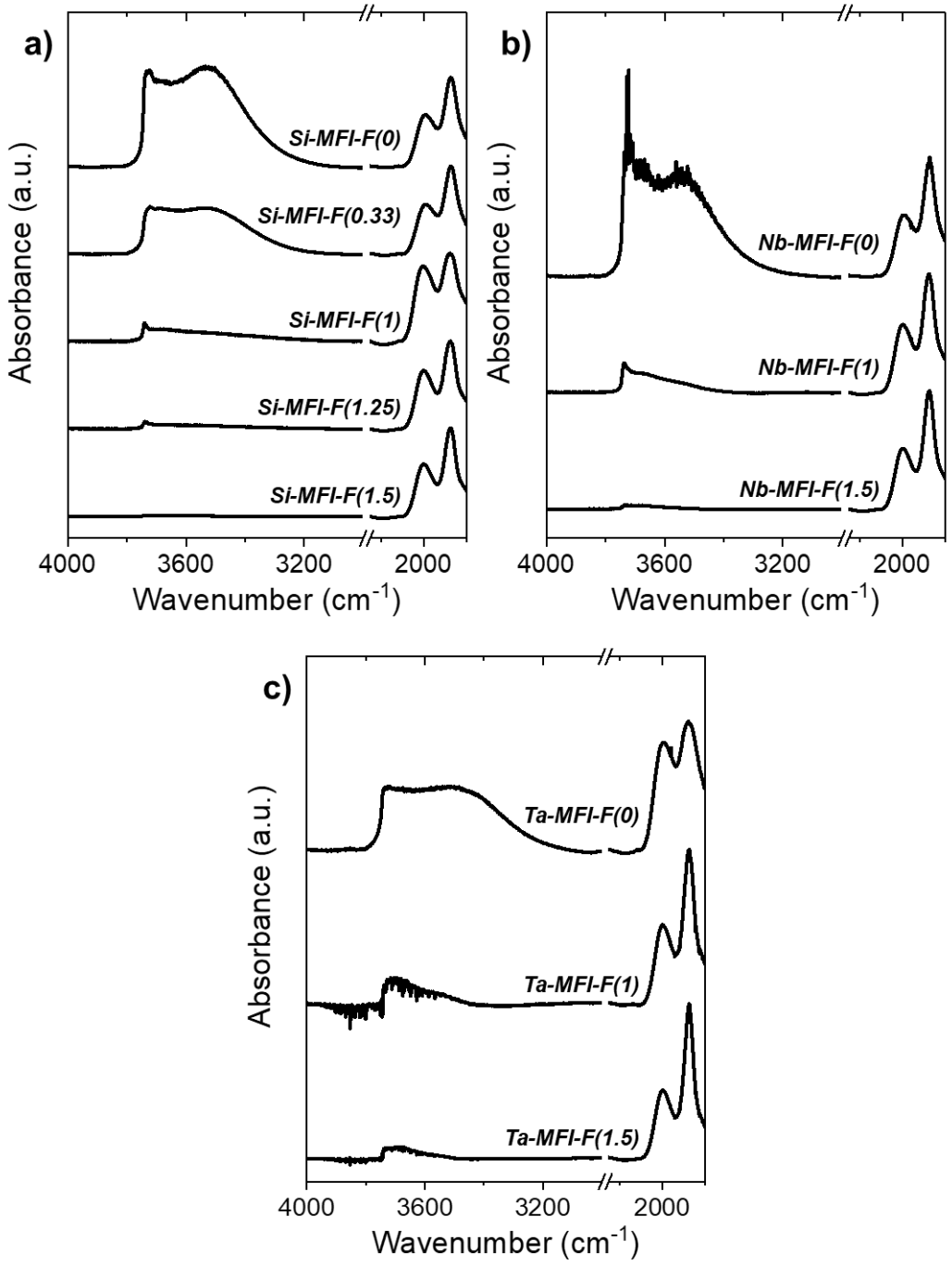

Figure S7. Infrared spectra of dehydrated a) Si-MFI-F(x), b) Nb-MFI-F(x), and Ta-MFI-F(x) at 573 K in flowing He (50 cm^3 min^{-1}). All spectra are normalized to the ν(Si-O-Si) overtone at 1865 cm^{-1} and are vertically offset for clarity.

Figure S7 shows a series of infrared (IR) spectra of Si, Nb-, and Ta-MFI-F(x) (x = 0, 0.33, 1, 1.25, or 1.5) at 573 K to desorb adsorbed volatile compounds. All spectra possess vibrational features at 1990 and 1865 cm^{-1} that correspond to ν(Si-O-Si) overtones from the MFI framework. The broad features between 3300 – 3750 cm^{-1} are attributed to ν(O-H) of the SiOH within these materials. The sharp feature at 3740 cm^{-1} corresponds to ν(O-H) of isolated SiOH, which do not interact with other SiOH species. The broad bimodal feature with peak centers at 3680 and 3540 cm^{-1} represents $(SiOH)_x$ groups that contain multiple, proximate hydrogen-bonded -OH functions.

S8. Metal Content within M-MFI-F(x) as a Function of HF to TPAOH Ratio

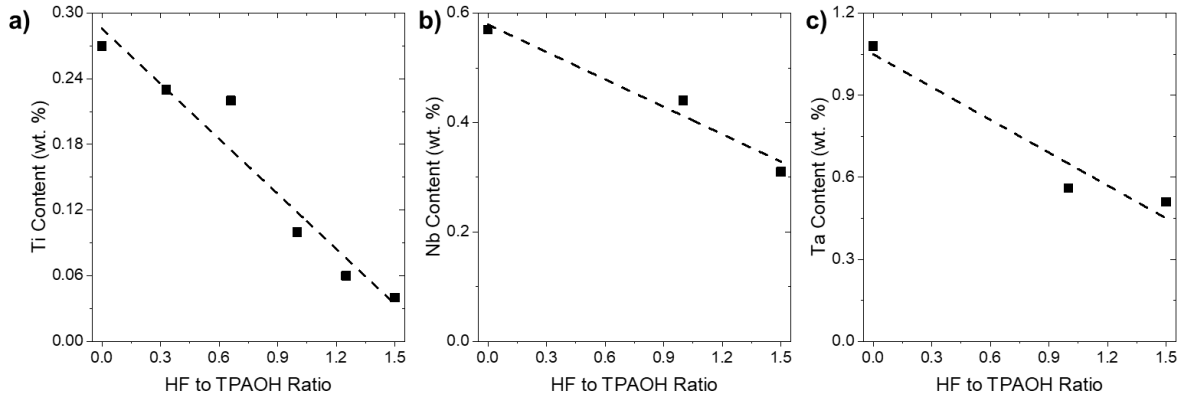

Figure S8. Metal content of a) Ti, b) Nb, and c) Ta within M-MFI-F(x) samples as a function of HF to TPAOH ratio. Ti-, Nb-, and Ta-MFI-F(x) samples were synthesized to contain 0.3 wt.% Ti, 0.6 wt. % Nb, or 1.2 wt.% Ta, respectively. Dashed lines represent linear fits.

The Ti, Nb, and Ta metal context within M-MFI-F(x) zeolites decreases linearly with the HF to TPAOH ratio within the synthesis gel, because HF condenses with $M(OH)_z$ complexes to form stable $M(OH)_xF_y$ species that are not incorporated into the MFI framework (Section 3.2).

S9. Raman Spectra of Supernatant from Ti- and Si-MFI-F(1.5) Syntheses

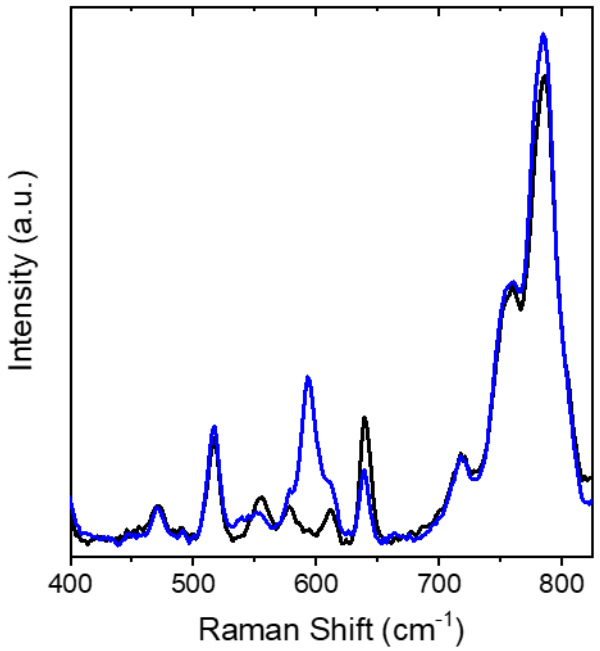

Figure S9. Raman spectra (λ_{ex} = 532 nm) of the dried supernatant from Si-MFI-F(1.5) (black) and Ti-MFI-F(1.5) (blue) syntheses.

Figure S9 shows Raman spectra of the dried supernatant from Ti- and Si-MFI-F(1.5) syntheses with an extended x-axis in comparison to Figure 7.

S10. H_2O Adsorption Isotherms within Nb-MFI-F(x)

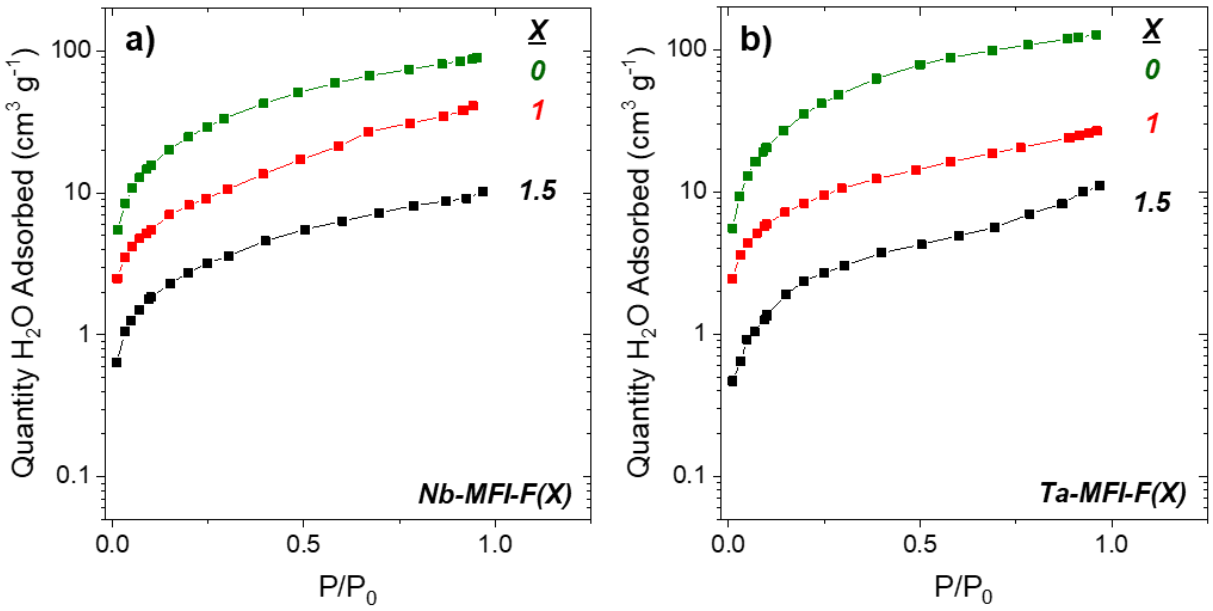

Figure S10. H_2O adsorption isotherms (293 K) within a) Nb-MFI-F(x) and b) Ta-MFI-F(x). Adsorption isotherms are *not* vertically offset.

Figure S10 shows H_2O adsorption isotherms for Nb- and Ta-MFI-F(0, 1, 1.5) resembles a type I isotherm. When the ratio of HF:TPAOH is increased from 0 to 1, there is 3-fold decrease in the amount of H_2O adsorbed. Further, the uptake of H_2O within M-MFI-F(0) is nearly 8-times greater than within M-MFI-F(1.5).

References:

1. Han, S. W.; Kim, J.; Ryoo, R., Dry-gel synthesis of mesoporous MFI zeolite nanosponges using a structure-directing surfactant. *Microporous Mesoporous Mater.* **2017,** *240*, 123-129.
2. Bregante, D. T.; Patel, A. Y.; Johnson, A. M.; Flaherty, D. W., Catalytic Thiophene Oxidation by Groups 4 and 5 Framework-Substituted Zeolites with Hydrogen Peroxide: Mechanistic and Spectroscopic Evidence for the Effects of Metal Lewis Acidity and Solvent Lewis Basicity. *J. Catal.* **2018,** *364*, 415-425.
3. Dzwigaj, S.; Millot, Y.; Méthivier, C.; Che, M., Incorporation of Nb(V) into BEA zeolite investigated by XRD, NMR, IR, DR UV–vis, and XPS. *Microporous Mesoporous Mater.* **2010,** *130*, 162-166.
4. Dutta, P. K.; Puri, M., Synthesis and Structure of Zeolite ZSM-5: A Raman Spectroscopic Study. *J. Phys. Chem.* **1987,** *91*, 4329-4333.
5. Frank, O.; Zukalova, M.; Laskova, B.; Kurti, J.; Koltai, J.; Kavan, L., Raman spectra of titanium dioxide (anatase, rutile) with identified oxygen isotopes (16, 17, 18). *Phys. Chem. Chem. Phys.* **2012,** *14*, 14567-14572.
6. Braga, V. S.; Dias, J. A.; Dias, S. C. L.; de Macedo, J. L., Catalyst Materials Based on Nb2O5 Supported on SiO2-Al2O3: Preparation and Structural Characterization. *Chem. Mater.* **2005,** *17*, 690-695.
7. Dobal, P. S.; Katiyar, R. S.; Jiand, Y.; Guo, R.; Bhalla, A. S., Raman scattering study of a phase transition in tantalum pentoxide. *J. Raman Spectr.* **2000,** *31*, 1061-1065.
8. Shannon, R. D., Revised Effective Ionic Radii and Systematic Studies of Interatomic Distances in Halides and Chalcogenides. *Acta Crystallographica* **1976,** *32*, 751-767.
9. Corma, A.; Llabre´s i Xamena, F. X.; Prestipino, C.; Renz, M.; Valencia, S., Water Resistant, Catalytically Active Nb and Ta Isolated Lewis Acid Sites, Homogeneously Distributed by Direct Synthesis in a Beta Zeolite. *J. Phys. Chem. C* **2009,** *113*, 11306-11315.
10. Bregante, D. T.; Tan, J. Z.; Sutrisno, A.; Flaherty, D. W., Heteroatom substituted zeolite FAU with ultralow Al contents for liquid-phase oxidation catalysis. *Catal. Sci. Tech.* **2020,** *10*, 635-647.